Nonmonotonic crossover and scaling behavior in a disordered one-dimensional quasicrystal

Anuradha Jagannathan,[1] Piyush Jeena,[2] and Marco Tarzia[3]

[1]*Laboratoire de Physique des Solides, CNRS-UMR 8502, Université Paris-Sud, 91405 Orsay, France*
[2]*Department of Physics, IIT Mumbai, Powai, Mumbai-400076, India*
[3]*LPTMC, CNRS-UMR 7600, Sorbonne Université, 4 Pl. Jussieu, F-75005 Paris, France*

We consider a noninteracting disordered 1D quasicrystal in the weak-disorder regime. We show that the critical states of the pure model approach strong localization in strikingly different ways, depending on their renormalization properties. A finite-size scaling analysis of the inverse participation ratios of states (IPR) of the quasicrystal shows that they are described by several kinds of scaling functions. While most states show a progressively increasing IPR as a function of the scaling variable, other states exhibit a nonmonotonic "reentrant" behavior wherein the IPR first decreases, and passes through a minimum, before increasing. This surprising behavior is explained in the framework of perturbation renormalization group treatment, where wave functions can be computed analytically as a function of the hopping amplitude ratio and the disorder, however it is not specific to this model. Our results should help to clarify results of recent studies of localization due to random and quasiperiodic potentials.

I. INTRODUCTION

It is established that, in many quasiperiodic models, electronic states are multifractal or "critical" in the absence of disorder [1–6]. The consequences of adding disorder to a quasiperiodic Hamiltonian have been studied as well, and rigorous arguments [7,8] predict that the addition of (uncorrelated short-range) disorder, however weak, will result in all states becoming localized. While this statement holds for infinite systems, in this paper, we consider *finite* samples (i.e., smaller than the localization length) to understand how critical states of the pure system change under addition of weak disorder. We will show that the answer to this question depends on the renormalization properties of the states, leading to different kinds of scaling functions for this problem. One motivation for our study comes from the recent experimental [9–14] and theoretical [15–19] work on many-body localization in interacting quasiperiodic systems where the question of differences in the nature of the transition for quasiperiodic (also called pseudorandom) versus random potentials has been raised [15–17].

In this paper, we consider the noninteracting model to show that interesting new phenomena can occur when random disorder is added to deterministic but nonperiodic order. Considering a tight-binding model on Fibonacci approximant chains in the weak-disorder regime where the chain length is much smaller than the putative localization length, we show that a large (but subextensive) set of states exhibit a nonmonotonic approach to strong localization. This implies that some states are initially delocalized, in the sense that their inverse participation ratio (IPR) starts to *decrease* with disorder. These states subsequently begin "relocalizing" when the disorder exceeds a certain value, as one expects, and as verified in other studies [20]. We speculate that this type of nonmonotonic behavior could occur in a generic way when the pure quasicrystal is perturbed.

The paper is organized as follows. Section II introduces the model. Section III describes the finite-size scaling analysis of the inverse participation ratio obtained from exact diagonalizations of disordered Fibonacci approximants. Section IV discusses the results obtained by perturbative renormalization group (RG) theory, with physical interpretation of the different scaling phenomena present. Finally, Sec. V gives a discussion of the results, along with perspectives.

II. HOPPING MODEL ON DISORDERED FIBONACCI CHAINS

The model considered here is a tight-binding problem of the following form:

$$H = \sum_i t_i(|i\rangle \langle i+1| + |i+1\rangle \langle i|). \qquad (1)$$

In this Hamiltonian, the hopping amplitudes $t_i = t_i^{(0)} + \epsilon_i$ are perturbed from the values $t_i^{(0)}$, the initial "pure" system hopping amplitudes which can take two values, t_A or t_B according to the deterministic Fibonacci sequence described below. The site energies are all assumed to be equal and can be set to zero by defining the origin suitably. The properties of the pure Hamiltonian depend on a *single* parameter, namely, the hopping ratio $\rho = t_A/t_B$ henceforward supposed to be in the range $0 \leqslant \rho \leqslant 1$ (in the following, we will set $t_B = 1$ without loss of generality). As customary in the Anderson localization literature, the random bond perturbations ϵ_i are chosen as independent and identically distributed (i.i.d.) random variables taken from a uniform distribution in the interval $[-W/2, W/2]$, such that $\langle \epsilon \rangle = 0$ and $\langle \epsilon^2 \rangle = W^2/12$. The value of W thus denotes the disorder strength. The sequence of hopping amplitudes t_A and t_B in the pure system corresponds to letters A and B of a specific series of chains leading in the infinite size limit to the Fibonacci quasicrystal.

These chains C_n, termed approximants, can be built iteratively by concatenation, namely $C_{n+1} = C_n C_{n-1}$. With initial conditions $C_0 = B$ and $C_1 = A$, the next few chains are AB, ABA, ABAAB, and so on. The lengths of these chains then obey the Fibonacci recursion relation $L_{n+1} = L_n + L_{n-1}$ with initial conditions $L_0 = L_1 = 1$, and the ratio of lengths of successive chains L_n/L_{n+1} tends to the (inverse) golden mean $\omega = (\sqrt{5} - 1)/2$, in the limit $n \to \infty$.

The properties of the pure model with no disorder ($\epsilon_j = 0 \, \forall j$) have been discussed in many classic papers, using a variety of methods, notably the powerful trace map method [3,4]. It is known that all states are delocalized in the sense of a vanishing Lyapunov exponent [2], but critical. Detailed information on spectrum and states have been obtained using the perturbative RG introduced by Niu and Nori and Kalugin *et al.* [21–23]. This approach gives quantitatively good predictions for the spectrum, eigenstates, and the quantum diffusion properties of wave packets for $\rho \ll 1$ [24–27]. We will extend this approach to the disordered case and use it to interpret our numerical results.

III. DISORDER DEPENDENCE AND FINITE-SIZE SCALING OF THE IPR

The averaged IPR corresponding to a given (normalized) eigenstate α ($\alpha = 1, \ldots, L$) as a function of the disorder strength W is defined by

$$\mathcal{I}_\alpha(W, L) = \left\langle \sum_{i=1}^{L} |\psi_\alpha(i)|^4 \right\rangle, \qquad (2)$$

where the brackets stand for the average over disorder. Throughout this paper we will label the states $|\alpha\rangle$ according to their increasing energies, such as $E_1 < E_2 < \ldots < E_L$, and we compare characteristics of states of given α for different system sizes, as fixed α corresponds to states of given RG path (as described in the next section). $\mathcal{I}$ is just one of the set of q moments of the probability of presence on each site. We consider the IPR ($q = 2$) in this paper, as an indicator of localization adequate for our noninteracting model (for interacting case see Ref. [28] for a discussion of the diagnostic tool involving the Kohn localization tensor). Recall that for large system size L, $\mathcal{I} \sim L^{-D_2}$ with D_2 having the value 1 for an extended state, 0 for a localized state and a value in-between for a critical state. In the Fibonacci chain approximants, the pure system IPR values $\mathcal{I}_\alpha(0, L_n)$ fluctuate irregularly in a self-similar fractal way with the index α. In the presence of disorder, the IPR evolve as illustrated in Fig. 1, which shows $\mathcal{I}$ as a function of W computed from exact diagonalizations of $n = 10$ chains (89 sites) for $\rho = 0.5$. Four different levels are shown to illustrate the different behaviors, which are seen. While the level at the lower band edge ($\alpha = 1$) shows a steep increase with W, others (such as $\alpha = 3$ and 7) show nonmonotonic behavior. The character strings in the figure are RG paths of each level, detailed in the next section.

As in the periodic model, the critical point corresponds to $W_c = 0$ (any disorder however weak localizes the critical states on the Fibonacci chain) with the localization length given by $\xi \sim W^{-\nu}$, where the ν is the correlation length exponent. In the weak-disorder regime, the IPR is expected
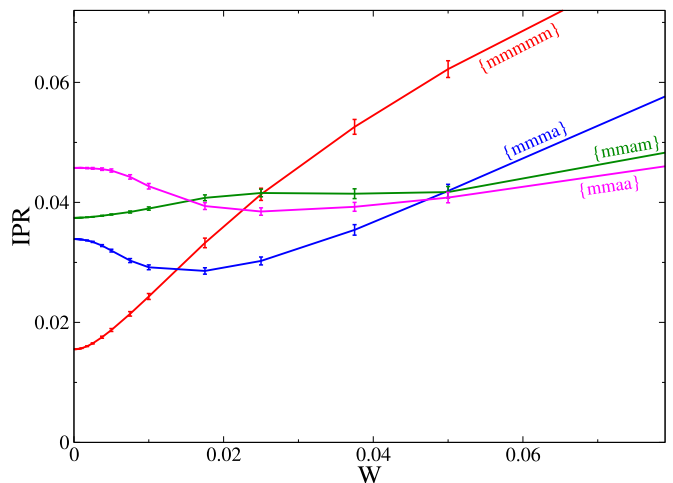

FIG. 1. Average IPR vs W for four states ($\alpha = 1$, red, $\alpha = 3$, blue, $\alpha = 7$, magenta, and $\alpha = 6$, green) on the $n = 10$ disordered chain ($L = 89$ and $t_A/t_B = 1/2$) obtained from exact diagonalizations (averages are performed over 262 144 independent disorder realizations). Level indices are indicated as are the RG paths (see text). The typical size of the IPR fluctuations is shown.

to have the scaling form

$$\frac{\mathcal{I}_\alpha(W, L)}{\mathcal{I}_\alpha(0, L)} = f_\alpha(L/\xi) \qquad (3)$$

(see Ref. [29] for a more general discussion of finite-size effects for the qth moments of wave functions near the critical point of the Anderson model). Scaling plots of the IPR obtained from exact diagonalizations for chains of generations $n = 10$ to $n = 16$ are presented in Fig. 2 for
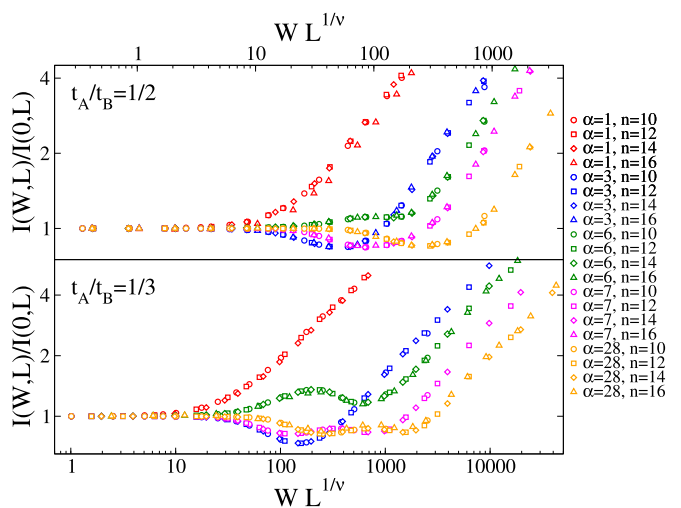

FIG. 2. Averaged IPR (normalized to $\mathcal{I}(0, L)$) of several states ($\alpha = 1, 3, 6, 7, 28$) and system sizes ($n = 10, 12, 14, 16$) and for $t_A/t_B = 1/2$ (top) and $t_A/t_B = 1/3$ (bottom) obtained from exact diagonalizations, showing data collapse as a function of the scaling variable $WL^{1/\nu}$ with $\nu = 1.7$ and 1.9, respectively. A similar behavior is found for all individual levels followed from one generation to the next. The nonmonotonicity of the IPR is more pronounced for smaller ρ and disappears continuously in the periodic limit ($\rho \to 1$).
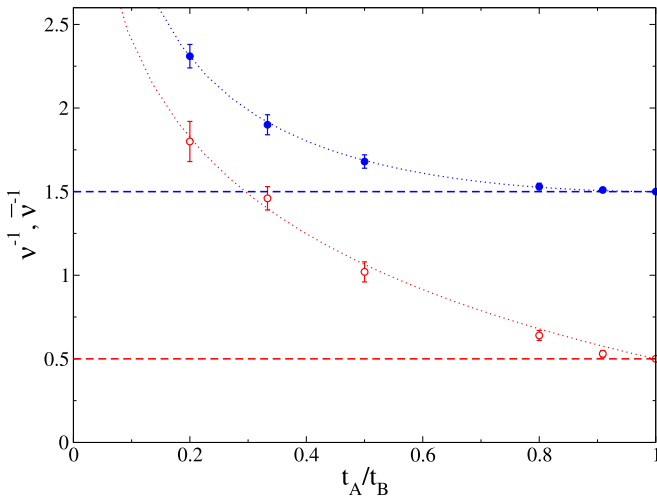
FIG. 3. Critical exponents ν and $\bar{\nu}$ as a function of the disorder plotted vs the ratio t_A/t_B. The horizontal dashed lines show the standard values of the exponents $\nu = 2/3$ and $\bar{\nu} = 2$ of the periodic system for the edge and the center states, respectively. The dashed lines represent logarithmic fits as $\nu^{-1} \simeq 3/2 + (-0.55 \ln \rho)^{1.74}$ and $\bar{\nu}^{-1} \simeq 1/2 - 0.82 \ln \rho$.

FIG. 4. (Top) Averaged IPR (normalized to $\mathcal{I}(0, L)$) of the center state ($\alpha = 1 + [L_n/2]$) for $n = 10$ (circles), 12 (squares), and 16 (diamonds) and for $t_A/t_B = 4/5$ (blue), 1/2 (red), and 1/3 (green) showing data collapse as a function of the scaling variable $WL^{0.5}$. (Bottom) IPR [normalized to] averaged over 1/16 of the states around $E = 0$ for $n = 10$ (circles), 12 (squares), 14 (diamonds), and 16 (up triangles) and for $t_A/t_B = 4/5$ (blue), 1/2 (red), and 1/3 (green) showing data collapse as a function of the scaling variable $WL^{1/\bar{\nu}}$.

$\rho = 1/2$ (top panel) and $\rho = 1/3$ (bottom panel), showing good collapse for *all* the states when $\mathcal{I}$ is plotted as a function of the scaling variable $WL^{1/\nu}$, for the values $\nu = 1.7 \pm 0.04$ and 1.9 ± 0.06, respectively (data are averaged over 262 144, 65 536, 12 288, and 2048 realizations for $n = 10, 12, 14,$ and 16, respectively). Several different scaling functions f_α are found, describing the variety of behaviors already seen in Fig. 1. Notice that our IPRs are defined with respect to a given state α followed from one generation to the next, implying that the energies of the states move towards the band edge as the system size is increased. We have checked numerically that the minima of the IPR of the states displaying the nonmonotonic behavior (as well as the wiggles and secondary minima of the other states) occur essentially when their energies start to cross with those of the neighboring levels (i.e., when the gaps become of the order of the fluctuations of energies), thereby suggesting that the changes of the behavior of the IPR are due to the onset of level repulsion.

Figure 3 shows the dependence of the nonuniversal exponent ν (blue filled circles) on the ratio of hopping amplitudes, ρ. The values of ν descend towards zero as ρ decreases, possibly logarithmically, to zero. However, this limit is difficult to study as some of the gaps between neighboring levels becomes extremely small leading to computational errors. In the periodic limit where $\rho = 1$, we find $\nu = 2/3$, in agreement with the result obtained for the disorder driven superfluid-insulator phase transition of noninteracting bosons [30]. This value corresponds, in that model as well, to scaling at the band edge. As noted by them, $\nu = 2/3$ violates the bound $\nu \geqslant 2/d$ established by Chayes *et al.* [31] for random (interacting) systems, as well as the generalized Harris-Luck criterion $\nu \geqslant 1/d$ [32] for aperiodic systems. This is not surprising since, unlike the present case, these inequalities apply to transitions at finite disorder. In fact, in contrast with the band edge
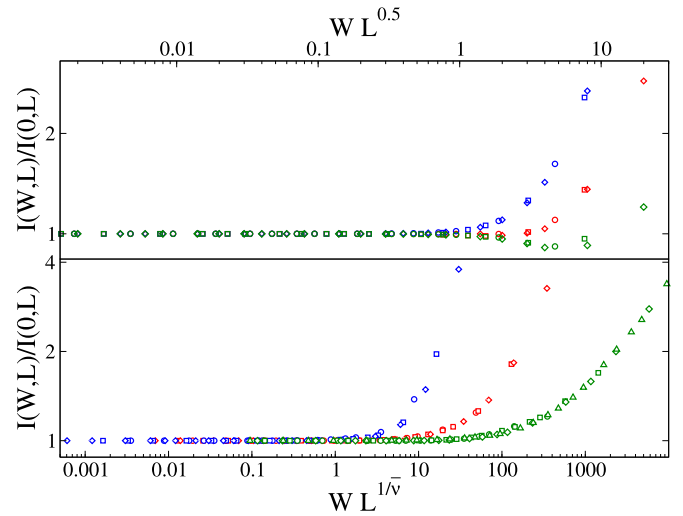
states, the state in the center of the spectrum at $\langle E \rangle = 0$ ($\alpha = 1 + [L_n/2]$ for L_n odd) scales with the standard universal exponent $\nu = 2$ for all hopping ratios ρ.

This is highlighted in the top panel of Fig. 4, which show the scaling plots of the IPR as a function of the disorder W of the state at the center of the spectrum. A good collapse of the data for several system sizes is found in terms of the scaling variable $WL^{1/2}$ for all values of ρ. Note that a nonmonotonicity of the IPR of the center state starts to appear for $\rho \lesssim 1/2$ and becomes more pronounced as ρ is further decreased.

One can also define quantities *averaged over states* in the vicinity of fixed energy or chemical potential. An analysis of finite-size scaling of the IPR at fixed energy $\langle E \rangle$ shows that it is described by a different (nonuniversal) exponent $\bar{\nu}$ for all values of E at fixed ρ. This is shown, for instance, in the bottom panel of Fig. 4, which exhibits the scaling plots of the IPR averaged over a small but finite fraction of the states around zero energy (in practice here we considered 1/16 of states around $\langle E \rangle = 0$). In this case, the data for several different sistem sizes show good collapse when plotted in terms of the scaling variable $WL^{1/\bar{\nu}}$. Note that no signs of the nonmonotonic behavior is seen in this case. The dependence of the exponent $\bar{\nu}$ on the ratio of hopping amplitudes is shown in Fig. 3 (red empty circles). We observe that $\bar{\nu}$ also decreases (possibly logarithmically) to zero as $\rho \to 0$ and approaches the standard value $\bar{\nu} = 2$ in the pure case, $\rho \to 1$. The same scaling exponent is found for other values of the energy $\langle E \rangle$ in the bulk of the spectrum (away from big gaps). This analysis underscores the importance of distinguishing between the different situations when analyzing a given experimental system.

IV. RG FOR PURE AND FOR WEAKLY DISORDERED CHAINS

We begin by briefly recall (for details see Refs. [27,33]) the steps of the real space RG for the pure system before discussing the addition of randomness. Sites on a given chain are termed either "molecule" sites—pairs of sites coupled via t_B—or "atom" sites—those with t_A on both sides. One defines two different real space decimation procedures: (i) decimating all atoms leaving only sites corresponding to molecules (mRG) or (ii) decimating all molecules leaving only the atom sites (aRG). To lowest nontrivial order in ρ one finds that under mRG, an initial chain C_n transforms to the chain C_{n-2}, with new weaker effective hopping amplitudes t_A' and t_B'. An energy shift of $\pm t_B$ (respectively, $-t_B$) occurs for bonding (m) and antibonding ($\overline{m}$) levels. Under aRG, an initial chain C_n transforms to the chain C_{n-3}, with new effective hopping amplitudes given by t_A'' and t_B''. The ratio of the strong and weak hopping amplitudes is left invariant in both types of RG. As a result the spectrum of the nth chain can be built up from the spectra of the $n-2$ and $n-3$ generation chains. For each energy level E_α ($\alpha = 1, \ldots, L_n$), one can define the "renormalization path" or set of characters $a, m, \overline{m}, \ldots$. Each element of this RG path is determined by whether the corresponding RG step was atomic or molecular. n_m denotes the total number of molecular RG steps, and n_a the overall number of atomic RG steps in the RG path. Figure 7(a) shows schematically how the spectra of chains $n = 4, 5$ are recursively obtained from spectra of smaller chains, along with the RG paths of levels. Figure 7(b) shows the spectra of two longer chains, with bands colored according to the last RG transformation (gray for $m(\overline{m})$ and red for a), in view of the discussion of the IPRs which will follow. Note that states having the same RG path terminations are expected to have similar properties on large length scales.

To each level described by some RG path, corresponds a wave function with support on sites having the *same* transformation properties under the RG. A wave function for energy E for a given chain can be related to the wave function of a state of energy E' on a smaller chain. The scale factors corresponding to mRG and aRG are denoted by λ and $\overline{\lambda}$ respectively, with $|\psi^{(n)}(i, E)|^2 = \lambda |\psi^{(n-2)}(i', E')|^2$ and $|\psi^{(n)}(i, E)|^2 = \overline{\lambda} |\psi^{(n-3)}(i', E')|^2$, where i and i' correspond to the site indices in the initial and final chains. The existence of two distinct scale factors λ and $\overline{\lambda}$ (functions of ρ [27]) leads to multifractality of the wave functions. These recursions relations imply that $\mathcal{I}(E, L_n) \sim L_n^{-D_2(E)}$ where the exponent $D_2(E)$ which measures the "mass scaling" of the atoms associated with the state of energy E depends on its RG path. An explicit calculation of $D_2(E)$ [26,27] shows that, in the limit $n \to \infty$, states at the edge of the spectrum (for which $n_m = n/2$) are "more extended", i.e., have a larger value of D_2, than the state in the center (for which $n_m = 0$).

A. Degenerate perturbation theory for disordered model

We now extend this RG scheme to our disordered model, for finite chains. We require that W be smaller than the smallest gaps of the spectrum ($W < \overline{z}^{n/3}$). This ensures that the branching hierarchical structure of the spectrum is conserved
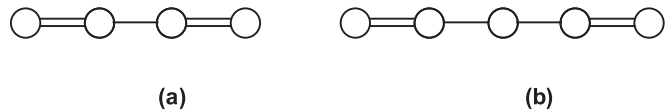

FIG. 5. (a) Cluster for strong bond calculation (mRG). (b) Cluster for weak bond calculation (mRG).

and the RG path structure of the pure system is not changed (no level crossing due to the random perturbation occurs). We aim to compute the renormalized hopping amplitudes, t_A' and t_B' obtained for a disordered Fibonacci chain in which the bonds have values of either $t_A + \epsilon_j$ (weak bond) or $t_A + \epsilon_j$ (strong bond). Although the on-site energies in the model are taken to be 0, diagonal terms will be generated under RG, and are denoted ξ_j, and we will also calculate their renormalized values. The zero-order Hamiltonian H_0 is off-diagonal, and consists only the pure strong couplings t_B, while the perturbation H_1 contains the weak bonds and diagonal on-site energy terms, ξ_j. In Brillouin-Wigner perturbation theory for degenerate states, the effective Hamiltonian is given by [22]

$$H_{\text{eff}} = QH_0Q + QH_1Q + QH_1P\frac{1}{E - H_0}PH_1Q + \ldots \quad (4)$$

in the subspace of energy E, where the operator $Q = \sum_\alpha |\psi_\alpha\rangle\langle\psi_\alpha|$ is the projection operator for states in this subspace, and $P = 1 - Q$.

We now illustrate the calculation of parameters of the effective Hamiltonian after a moleculer RG (mRG), namely, the on-site energies ξ', and the renormalized strong and weak couplings t_B', t_A'. Figure 5(a) shows the cluster of sites which renormalize to give a strong bond after mRG. The three bonds are $t_B + \epsilon_1$, $t_A + \epsilon_2$ and $t_B + \epsilon_3$. The on-site energies are zero in the first RG step, but subsequently acquire nonzero values, which are denoted by ξ_j ($j = 1$ to 3). The eigenstates of H_0 are $|\psi_1\rangle = (|1\rangle + |2\rangle)/\sqrt{2}$, $|\psi_2\rangle = (|3\rangle + |4\rangle)/\sqrt{2}$, corresponding to $E = t_B$, and $|\psi_3\rangle = (|1\rangle - |2\rangle)/\sqrt{2}$, and $|\psi_4\rangle = (|3\rangle - |4\rangle)/\sqrt{2}$, corresponding to $E = -t_B$.

Using Eq. (4), the on-site energy for the leftmost molecular bonding state, is, to lowest nonvanishing order

$$\xi_1' = \langle\psi_1|H_{\text{eff}}|\psi_1\rangle = \tfrac{1}{2}(\xi_1 + \xi_2) + \epsilon_1, \quad (5)$$

with a similar result for the on-site energy for the right molecular state. The effective (strong) hopping amplitude between the two bonding molecular states is

$$t_B' \equiv \langle\psi_1|H_{\text{eff}}|\psi_2\rangle = \tfrac{1}{2}(t_A + \epsilon_2). \quad (6)$$

The renormalized weak coupling is found by considering the cluster in Fig. 5(b) consisting of five sites. The eigenstates of H_0 are now $|\psi_1\rangle = (|1\rangle + |2\rangle)/\sqrt{2}$, $|\psi_2\rangle = (|4\rangle + |5\rangle)/\sqrt{2}$, corresponding to $E = t_B$, $|\psi_3\rangle = |3\rangle$, $|\psi_4\rangle = (|1\rangle - |2\rangle)/\sqrt{2}$, and $|\psi_5\rangle = (|4\rangle - |5\rangle)/\sqrt{2}$, corresponding to $E = -t_B$. The effective (weak) hopping amplitude is of second order:

$$t_A' \equiv \langle\psi_1|H_{\text{eff}}|\psi_2\rangle = \frac{1}{2t_B}(t_A + \epsilon_2)(t_A + \epsilon_3). \quad (7)$$

For atomic RG, the clusters to consider for the new strong and weak amplitudes are shown in Fig. 6. The on-site energy and strong and weak hopping amplitudes after aRG are found
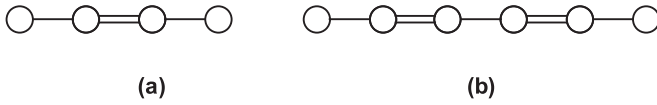
FIG. 6. (a) Cluster for strong bond calculation (aRG). (b) Cluster for weak bond calculation (aRG).

to be

$$\xi_1' = \xi_1 \, ,$$
$$t_B' = -(t_A + \epsilon_1)(t_A + \epsilon_3)/t_B \, ,$$
$$t_A' = (t_A + \epsilon_1)(t_A + \epsilon_3)(t_A + \epsilon_5)/t_B^2 \, . \quad (8)$$

The results of the degenerate perturbation theory, obtained in Eqs. (5)–(8) in the limit of small W, are summarized in the table below, which gives the on-site energy and the hopping amplitudes up to second order in the perturbations after the first RG step:

	mRG	aRG
ξ_i	ϵ	0
t_B'	$\frac{(t_A+\epsilon)}{2}$	$-\frac{(t_A+\epsilon)(t_A+\epsilon')}{t_B}$
t_A'	$\frac{(t_A+\epsilon)(t_A+\epsilon')}{t_B}$	$\frac{(t_A+\epsilon)(t_A+\epsilon')(t_A+\epsilon'')}{t_B^2}$

(9)

where as already stated, the ϵ are i.i.d. random variables.

Disordering the Fibonacci chain therefore leads to small on-site energy corrections ξ_i (zero for aRG at this order) and modified renormalized hopping amplitudes. From Eqs. (9), one sees that the average renormalized hopping amplitudes are unchanged from their pure values, but their variance is proportional to W^2. The spectrum is broadened—i.e., while the average value or center of mass of minibands of the chain are not shifted at lowest order, their widths increase with the disorder strength. For W small enough that levels do not overlap, the RG can therefore proceed as in the pure case. wave functions are determined by the coupling ratio, whose average value is renormalized to $\rho' = \rho + W^2$ and therefore increases under RG. Since small ρ corresponds to stronger quasiperiodic modulation, one observes that the disorder diminishes the quasiperiodic modulation—as the number of RG steps increases one gets a homogeneously disordered chain in the large distance limit.

For strong values of disorder gaps are filled in progressively, with the two largest gaps of width $\sim t_B - t_A$ being the last to disappear (when W becomes of the order of t_B). At large disorder, the familiar form of the DOS well-known in the literature of the off-diagonal 1D Anderson model (as reviewed in Ref. [34]) is recovered.

B. IPR corrections due to disorder

The different types of IPR scaling functions seen in Figs. 1 and 2 can now be explained in terms of the nature of the level after the last RG step. As can be seen from Fig. 7(b) the number of "red" levels doubles with each mRG so that for large n, the number of red levels grows as $2^{n/2}$. The total number of levels grows as $L \sim \omega^{-n}$, so the number of the nonmonotonic "atom" states grows with the system size as L^β,
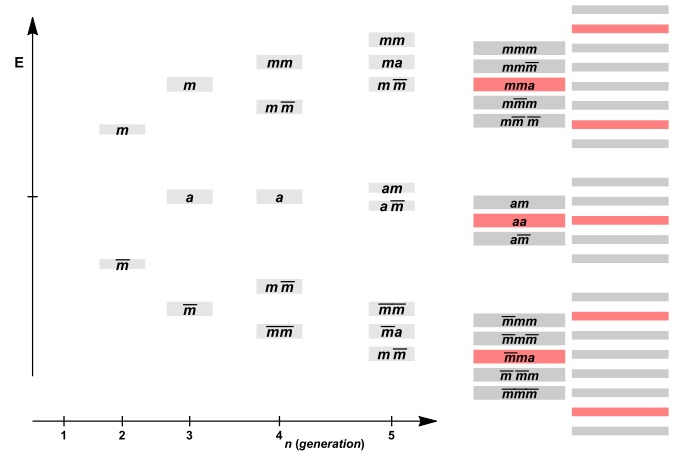

FIG. 7. (a) Spectra (in arbitrary units) for successive generations of approximants, showing the recursive structure in RG. (b) The left figure shows the spectrum of a 13-site chain, on the right, the spectrum of a 21-site chain. Bands are colored according to the last RG step: molecular (gray) or atom (red),

with $\beta = \ln 2/(2\ln(1/\omega)) \simeq 0.72$. The red levels are those which show a negative IPR change as we will explain below. Considering all combinations of m and a states in the last RG step, we have four possible situations. These four classes of levels have wave functions with support on sites which have the same RG characteristics—these are shown in the inset of Fig. 8 along with the final form (molecule or atom). The strong bonds (represented by double lines) of each cluster are taken to be $t_B + \epsilon_j$ and the weak bonds (single lines) are $t_A + \epsilon_j$. The variation of the IPR, $\Delta\mathcal{I}$, can be found by diagonalizing the pure Hamiltonian as a function of ρ, computing wave-function corrections in standard second-order perturbation theory in ϵ_j, and finally averaging over all random variables of the cluster.

In order to do this, we consider the hopping model of Eq. (1), where each of the hopping terms is either a perturbed
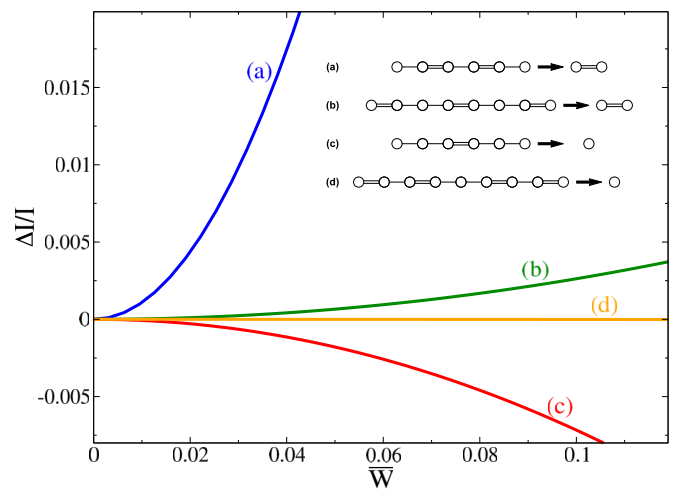

FIG. 8. Plots of $\Delta\mathcal{I}(W)/\mathcal{I}(0)$ for $\rho = 0.46$ using the expressions given in Eq. (10). (Inset) Clusters transforming to final molecular state (a) via mRG and (b) via aRG and clusters transforming to final atomic state (c) via mRG and (d) via aRG.

strong ($t_B + \epsilon_j$) or perturbed weak ($t_A + \epsilon_j$) bond, where ϵ_j are i.i.d. variables uniformly distributed in $[-W/2, W/2]$. In the pure system, the wave functions corresponding to the levels of interest have their support primarily (for small ρ) on specific groups of sites arranged as in the four clusters shown in the inset of Fig. 8. Weak disorder leads to a small redistribution of amplitudes, that we want to compute, perturbatively. We will be interested in the IPR change of specific states: the band edge molecular level $\alpha = 1$ for clusters (a) and (b), and in the atom level close to/at the center for the clusters (c) and (d). The full Hamiltonian is off-diagonal, with L sites and $L - 1$ bonds. The latter can be strong or weak bonds, with weak disorder in each of the hopping amplitudes, as given in Eq. (1). The aim of the calculations is to compute the changes of IPR due to the disorder for specific states on each of the clusters, using second-order perturbation theory.

As contrasted with the Brillouin-Wigner perturbation expansion for degenerate states, here we will proceed by splitting the Hamiltonian differently as follows: $H = H_F + H_d$, where the Fibonacci Hamiltonian H_F includes the pure strong and weak bonds (t_B and t_A), and H_d contains the disordered part, ϵ_j. For a given cluster of L sites, the normalized eigenstates of H_F, denoted by $\{|\psi_\alpha\rangle\}$ (with $\alpha = 1, \ldots, L$) are nondegenerate and can be computed exactly as a function of $\rho = t_A/t_B$. For each of the clusters the IPR of the state α at zero order of the perturbation is then given by $\mathcal{I}(0) = \sum_i |\psi_\alpha(i)|^4$.

Using standard perturbation theory, the first- and second-order corrections to the wave function are

$$|\psi_\alpha\rangle^{(1)} = \sum_{\beta \neq \alpha} \frac{\langle\psi_\beta|H_d|\psi_\alpha\rangle}{E_\alpha - E_\beta} |\psi_\beta\rangle \,,$$

$$|\psi_\alpha\rangle^{(2)} = \sum_{\beta \neq \alpha} \left[-\frac{\langle\psi_\alpha|H_d|\psi_\alpha\rangle\langle\psi_\beta|H_d|\psi_\alpha\rangle}{(E_\alpha - E_\beta)^2} \right.$$
$$\left. + \sum_{\gamma \neq \alpha} \frac{\langle\psi_\beta|H_d|\psi_\gamma\rangle\langle\psi_\gamma|H_d|\psi_\alpha\rangle}{(E_\alpha - E_\beta)(E_\alpha - E_\gamma)} \right] |\psi_\beta\rangle \,,$$

which are combined with the zeroth-order term to give $|\psi_\alpha'\rangle$. The new IPR is then given by $\mathcal{I}' = \sum_i |\psi_\alpha'(i)|^4 / (\sum_i |\psi_\alpha'(i)|^2)^2$. As there is no convenient closed form expression as a function of ρ for the fractional change defined by $\Delta\mathcal{I}/\mathcal{I}(0) = (\mathcal{I}' - \mathcal{I}(0))/\mathcal{I}(0)$, we will present the results for each of the four states in terms of an expansion around a point $\rho = \rho_0$.

(a) $\quad \dfrac{\Delta\mathcal{I}}{\mathcal{I}(0)} \simeq [11.32 - 43.83\,\delta\rho + 147.12(\delta\rho)^2]\tilde{W}^2 \,,$

(b) $\quad \dfrac{\Delta\mathcal{I}}{\mathcal{I}(0)} \simeq [0.15 + 10.98\,\delta\rho - 4.11(\delta\rho)^2]\tilde{W}^2 \,,$

(c) $\quad \dfrac{\Delta\mathcal{I}}{\mathcal{I}(0)} \simeq [-0.77 + 5.25\,\delta\rho + 10.19(\delta\rho)^2]\tilde{W}^2 \,,$

(d) $\quad \dfrac{\Delta\mathcal{I}}{\mathcal{I}(0)} \simeq [-0.14 + 13.6\,\delta\rho + 3.22(\delta\rho)^2]\tilde{W}^2 \,,$ (10)

with $\delta\rho = \rho - \rho_0$, for $\rho_0 = 0.45$. In these expressions, $\tilde{W}$ denotes the width of effective renormalized distribution, which increases with the number of RG steps. Figure 8 shows plots of these four functions for $\rho = 0.46$. They provide qualitative
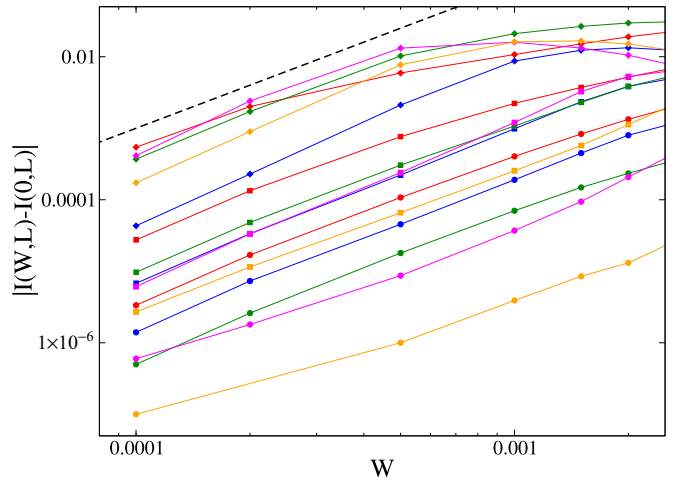

FIG. 9. Log-log plot of $\mathcal{I}_\alpha(W, L) - \mathcal{I}_\alpha(W, 0)$ as a function of the disorder strength W in the $W \to 0$ region for $n = 12$ ($L = 233$), for several states, $\alpha = 1$ (red), 3 (blue), 6 (green), 7 (magenta), and 28 (orange), and for several values of the ratio t_A/t_B, $\rho = 1/2$ (squares), $1/3$ (circles), and $1/5$ (diamond). The dashed line correspond to a quadratic function.

indications of the behavior of these states since the theory is quantitatively accurate only for values $\rho \ll 1$.

Exact diagonalization results confirm that the IPR of all levels depends quadratically on the disorder for $W \to 0$. In particular, in Fig. 9, we show the results of exact diagonalizations for $|\mathcal{I}_\alpha(W, L) - \mathcal{I}_\alpha(W, 0)|$ as a function of W in the small disorder region for $n = 12$ ($L = 233$) and for several states (the same as Fig. 2) and three different values of ρ. This plot confirms that the IPR of all states behaves quadratically for $W \to 0$ as

$$\mathcal{I}_\alpha(W, L_n) \simeq \mathcal{I}_\alpha(0, L_n) + c_\alpha^{(n)} W^2 \,,$$

with positive or negative coefficients $c_\alpha^{(n)}$ depending on the level index (e.g., $c_\alpha^{(n)} < 0$ for $\alpha = 3, 7, 11, 15, 20, 24, 28, 32, 36, \ldots$). This is precisely the behavior predicted by the real space RG approach [see Eq. (5) of the main text].

Comparing with the $W \to 0$ regime of Fig. 1, these results for the curvature correspond to the initial behavior of the curves: levels of type (a) and (b) corresponding to molecular final states have positive curvatures, while (c) and (d) corresponding to atomic final states have negative curvatures. Case (a) describes band edge states, which localize the most rapidly as disorder is increased compared to the other curves. More differences between levels will appear when longer-range structural information is included. These results are not qualitatively changed upon adding on-site randomness.

The sign of the IPR change can be explained in terms of a very simple general argument which is not restricted to the specific case of the Fibonacci chain, as shown schematically in Fig 10. When the wave function in the pure systems is maximally delocalized, as for the m state (top figure), disorder tends to *increase* the IPR—as seen from the change of the wave function. When on the other hand the initial wave function is maximally localized (as for the atom state in the lower figure), disorder leads to a *decrease* of the IPR.
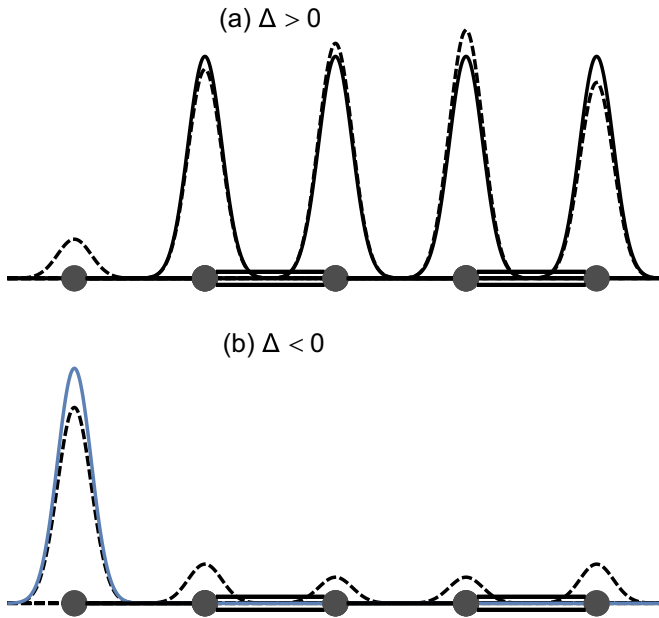
FIG. 10. Schemas for two kinds of wave functions (a) molecular wave function for pure (continuous) and weakly disordered (dashed) chain. (b) Atom wave functions before and after adding weak disorder. Δ, the change of the IPR, is positive (respectively, negative) for the two cases.

To repeat, the behavior shown in Fig. 8 is expected only for very small disorder. For large W, differences between "strong" and "weak" bonds cease to exist and the standard Anderson model is recovered, in which the IPR increases with W (as discussed above, this occurs when the disorder strength becomes of the order of the gaps with the neighboring states and level repulsion sets in). The negative-curvature of $\Delta(\mathcal{I})/\mathcal{I}$ will therefore eventually "bottom out" and start increasing with W, as we saw in Fig. 2. [Notice that the IPR of all the states tend to $1/2$ in the $W \to \infty$ limit for the model described by the Hamiltonian (1).]

V. CONCLUSIONS AND DISCUSSION

To sum up, we have shown, by considering finite approximants of the Fibonacci chain, that the addition of disorder in a model with critical states can lead to an effect of delocalization followed by localization of a subset of levels. We have presented an argument to explain the disorder-dependence of IPR for levels as a function of their RG path. We stress that this phenomenon is not restricted to this specific model [35,36], however in the Fibonacci chain one can predict the total number and the energies of such states thanks to the underlying RG scheme.

The states which exhibit nonmonotonic behavior are those which under RG ultimately are reduced to a single "atom" level ($\alpha = 3, 7, 11, 15, 20, 24, 28, 32, 36, \ldots$), while the other levels show the expected monotonic increase of the IPR with W. The number of the nonmonotonic "atom" states grows with the system size as L^β, with $\beta \simeq 0.72$. For stronger values of disorder, an upturn of the curves will eventually occur, as the localization lengths become smaller than the

chain length, and the usual Anderson localization physics is recovered. The exponent ν describing the approach to strong localization depends on the parameter ρ, tending to very small values for $\rho \to 0$, beyond the region of reliability of the numerical computations. The scaling functions for the IPR are different according to the nature of the level (and some of them are nonmonotonic). These characteristics show that this localization transition is in a different universality class from the standard Anderson model, which is recovered in the limit $\rho = 1$, with the value $\nu = 2/3$ as found previously in a different context [30]. A similar result has been recently found in Ref. [35] where it was shown that Anderson localization in a 2D generalization of the Aubry-André model appears to be in a quite different universality class from the same model with random potentials.

Some works [37,38] incorporate geometrical forms of disorder where segments of the chains are flipped. From analyzing Lyapunov exponents using RG [38] and by direct transfer matrix methods, it was concluded that localization does not occur in this case. More detailed finite-size scaling analyses of the phason disordered 1D Fibonacci chains are probably necessary before this issue can be definitively settled. In this context, we note that a similar type of geometrical disorder is considered in a 2D model, and shown to lead to localization of the ground state [39].

The reentrant delocalization localization of certain states could also be observable in experiments on multilayer systems, by means of precise measurements of the transport in mesoscopic samples. In this context it can be noted that, for three-dimensional quasicrystals such as AlCuFe, it was long ago pointed out that structural disorder tends to *improve* conductivity [40].

Our results can be expected to have relevance for the debate on many-body localization due to disorder versus localization due to pseudodisorder [15–19]. It was indeed observed that, contrary to naive expectations, adding interactions in quasiperiodic systems does not enhance delocalization, and a MBL transition is observed both in Fibonacci spin chains [19] and in fermionic Aubry-André models [18]. Our results suggest that the transition might have an intermediate regime, where finite-size effects can be anomalous. Generally speaking, adding perturbations to the pure noninteracting Hamiltonian could produce nonmonotonic or reentrant behavior. Questions concerning the critical properties for each case are not just theoretical problems, but are now amenable to experimental verification using cold atoms [9–14].

Many important theoretical questions remain open. One concerns the robustness of our findings with respect to the nature of the quenched disorder. As discussed above, it seems reasonable to expect that the addition of i.i.d. on-site disorder to the Hamiltonian does not modify the results as this leaves qualitatively unchanged the RG transformations. In the same spirit, one could wonder whether the choice of a Gaussian distribution of the random hoppings ϵ_i might alter the scenario discussed here. Although in the context of Anderson localization taking a Gaussian versus a box distribution leads essentially to the same physical picture, this is an interesting question, since for unbounded ϵ_i's level crossing is not

forbidden even at infinitesimal disorder and the RG path of neighboring levels might get mixed. Heavy-tailed and/or correlated randomness, instead, are expected to alter significantly the present scenario. Another very interesting research direction is to consider other kinds of random perturbation to the Fibonacci approximants. Preliminary results indicates that the same kind of nonmonotonic behavior of the IPR is observed for the same states (the atomic final states) as for the disordered case in a model where few weak long-range matrix elements are added the pure Hamiltonian (1)—thereby transforming the 1D chain into a sparse random matrix with a Fibonacci backbone—suggesting that the way in which individual levels respond to perturbations might be a specific (and robust) feature of their individual critical properties. Finally, it would also be interesting to investigate the region of the phase diagram $t_A > t_B$ ($\rho > 1$) for which much less is known even in the pure limit.

After this paper was submitted, numerical results have been reported for a different quasiperiodic model – the Harper model [36], for which the authors report nonmonotonic length dependence of the transport and consequent failure of single parameter scaling. Their results, for 1D in particular, complement our findings for the Fibonacci model and extend the studies to higher dimensions. It will be interesting to study in detail similarities and differences between the two families of quasiperiodic models.

[1] S. Ostlund, R. Pandit, D. Rand, H. J. Schellnhuber, and E. D. Siggia, Phys. Rev. Lett. **50**, 1873 (1983).

[2] F. Delyon and D. Petritis, Commun. Math. Phys. **103**, 441 (1986).

[3] M. Kohmoto, L. P. Kadanoff, and C. Tang, Phys. Rev. Lett. **50**, 1870 (1983).

[4] M. Kohmoto, B. Sutherland, and C. Tang, Phys. Rev. B **35**, 1020 (1987).

[5] C. Tang and M. Kohmoto, Phys. Rev. B **34**, 2041 (1986).

[6] H. H. Hiramoto and M. Kohmoto, Phys. Rev. B **40**, 8225 (1989).

[7] F. Delyon, Y.-E. Lévy, and B. Souillard, Phys. Rev. Lett. **55**, 618 (1985).

[8] S. Kotani and B. Simon, Commun. Math. Phys. **112**, 103 (1987).

[9] M. Schreiber, S. S. Hodgman, P. Bordia, H. P. Luschen, M. H. Fischer, R. Vosk, E. Altman, U. Schneider, and I. Bloch, Science **349**, 842 (2015).

[10] H. P. Lüschen, P. Bordia, S. Scherg, F. Alet, E. Altman, U. Schneider, and I. Bloch, Phys. Rev. Lett. **119**, 260401 (2017).

[11] P. Bordia, H. P. Lüschen, S. Scherg, S. Gopalakrishnan, M. Knap, U. Schneider, and I. Bloch, Phys. Rev. X **7**, 041047 (2017).

[12] P. Bordia, H. P. Lüschen, S. S. Hodgman, M. Schreiber, I. Bloch, and U. Schneider, Phys. Rev. Lett. **116**, 140401 (2016).

[13] B. Deissler, M. Zaccanti, G. Roati, C. D'Errico, M. Fattori, M. Modugno, G. Modugno, and M. Inguscio, Nat. Phys. **6**, 354 (2010).

[14] J. Hou, H. Hu, K. Sun, and C. Zhang, Phys. Rev. Lett. **120**, 060407 (2018).

[15] S. Iyer, V. Oganesyan, G. Refael, and D. A. Huse, Phys. Rev. B **87**, 134202 (2013).

[16] M. Lee, T. R. Look, S. P. Lim, and D. N. Sheng, Phys. Rev. B **96**, 075146 (2017).

[17] V. Khemani, D. N. Sheng, and D. A. Huse, Phys. Rev. Lett. **119**, 075702 (2017).

[18] Y. Bar Lev, D. M. Kennes, C. Klöckner, D. R. Reichman, and C. Karrasch, Europhys. Lett. **119**, 37003 (2017).

[19] N. Macé, N. Laflorencie, and F. Alet, arXiv:1811.01912.

[20] Y. Liu and R. Riklund, Phys. Rev. B **35**, 6034 (1987).

[21] Q. Niu and F. Nori, Phys. Rev. Lett. **57**, 2057 (1986).

[22] Q. Niu and F. Nori, Phys. Rev. B **42**, 10329 (1990).

[23] P. A. Kalugin, A. Yu. Kitaev, and L. S. Levitov, ZhETF **91**, 692 (1986) [Sov. Phys. JETP **64**, 410 (1986)].

[24] F. Piéchon, M. Benakli, and A. Jagannathan, Phys. Rev. Lett. **74**, 5248 (1995).

[25] F. Piéchon, Phys. Rev. Lett. **76**, 4372 (1996).

[26] S. Thiem and M. Schreiber, J. Phys.: Condens. Matter **25**, 075503 (2013).

[27] N. Macé, A. Jagannathan, and F. Piéchon, Phys. Rev. B **93**, 205153 (2016).

[28] V. K. Varma, S. Pilati, and V. E. Kravtsov, Phys. Rev. B **94**, 214204 (2016).

[29] A. Rodriguez, L. J. Vasquez, K. Slevin, and R. A. Römer, Phys. Rev. B **84**, 134209 (2011).

[30] J. C. C. Cestari, A. Foerster, M. A. Gusmão, and M. Continentino, Phys. Rev. A **84**, 055601 (2011).

[31] J. T. Chayes, L. Chayes, D. S. Fisher, and T. Spencer, Phys. Rev. Lett. **57**, 2999 (1986).

[32] J. M. Luck, Europhys. Lett. **24**, 359 (1993).

[33] S. Thiem and M. Schreiber, Phys. Rev. B **85**, 224205 (2012).

[34] B. Kramer and A. MacKinnon, Rep. Prog. Phys. **56**, 1469 (1993).

[35] T. Devakul and D. A. Huse, Phys. Rev. B **96**, 214201 (2017).

[36] J. Sutradhar, S. Mukerjee, R. Pandit, and S. Banerjee, arXiv:1810.12931.

[37] D. Huang and D. Huang, Phys. Rev. B **70**, 205124 (2004).

[38] M. T. Velhinho and I. R. Pimentel, Phys. Rev. B **61**, 1043 (2000).

[39] J.-N. Fuchs and J. Vidal, Phys. Rev. B **94**, 205437 (2016).

[40] D. Mayou, C. Berger, F. Cyrot-Lackmann, T. Klein, and P. Lanco, Phys. Rev. Lett. **70**, 3915 (1993).